NASA/TM—2013-216603

Absolute Thickness Measurements on Coatings Without Prior Knowledge of Material Properties Using Terahertz Energy

Donald J. Roth
Glenn Research Center, Cleveland, Ohio

Laura M. Cosgriff
Consultant, Lakewood, Ohio

Bryan Harder and Dongming Zhu
Glenn Research Center, Cleveland, Ohio

Richard E. Martin
Cleveland State University, Cleveland, Ohio

December 2013

NASA STI Program . . . in Profile

Since its founding, NASA has been dedicated to the advancement of aeronautics and space science. The NASA Scientific and Technical Information (STI) program plays a key part in helping NASA maintain this important role.

The NASA STI Program operates under the auspices of the Agency Chief Information Officer. It collects, organizes, provides for archiving, and disseminates NASA's STI. The NASA STI program provides access to the NASA Aeronautics and Space Database and its public interface, the NASA Technical Reports Server, thus providing one of the largest collections of aeronautical and space science STI in the world. Results are published in both non-NASA channels and by NASA in the NASA STI Report Series, which includes the following report types:

- TECHNICAL PUBLICATION. Reports of completed research or a major significant phase of research that present the results of NASA programs and include extensive data or theoretical analysis. Includes compilations of significant scientific and technical data and information deemed to be of continuing reference value. NASA counterpart of peer-reviewed formal professional papers but has less stringent limitations on manuscript length and extent of graphic presentations.

- TECHNICAL MEMORANDUM. Scientific and technical findings that are preliminary or of specialized interest, e.g., quick release reports, working papers, and bibliographies that contain minimal annotation. Does not contain extensive analysis.

- CONTRACTOR REPORT. Scientific and technical findings by NASA-sponsored contractors and grantees.

- CONFERENCE PUBLICATION. Collected papers from scientific and technical conferences, symposia, seminars, or other meetings sponsored or cosponsored by NASA.

- SPECIAL PUBLICATION. Scientific, technical, or historical information from NASA programs, projects, and missions, often concerned with subjects having substantial public interest.

- TECHNICAL TRANSLATION. English-language translations of foreign scientific and technical material pertinent to NASA's mission.

Specialized services also include creating custom thesauri, building customized databases, organizing and publishing research results.

For more information about the NASA STI program, see the following:

- Access the NASA STI program home page at *http://www.sti.nasa.gov*

- E-mail your question to *help@sti.nasa.gov*

- Fax your question to the NASA STI Information Desk at 443–757–5803

- Phone the NASA STI Information Desk at 443–757–5802

- Write to:
  STI Information Desk
  NASA Center for AeroSpace Information
  7115 Standard Drive
  Hanover, MD 21076–1320

NASA/TM—2013-216603

Absolute Thickness Measurements on Coatings Without Prior Knowledge of Material Properties Using Terahertz Energy

Donald J. Roth
Glenn Research Center, Cleveland, Ohio

Laura M. Cosgriff
Consultant, Lakewood, Ohio

Bryan Harder and Dongming Zhu
Glenn Research Center, Cleveland, Ohio

Richard E. Martin
Cleveland State University, Cleveland, Ohio

National Aeronautics and
Space Administration

Glenn Research Center
Cleveland, Ohio 44135

December 2013

Acknowledgments

This work was sponsored by code Q, NASA Nondestructive Evaluation Working Group.

Level of Review: This material has been technically reviewed by technical management.

Available from

NASA Center for Aerospace Information
7115 Standard Drive
Hanover, MD 21076–1320

National Technical Information Service
5301 Shawnee Road
Alexandria, VA 22312

Available electronically at http://www.sti.nasa.gov

Absolute Thickness Measurements on Coatings Without Prior Knowledge of Material Properties Using Terahertz Energy

Donald J. Roth
National Aeronautics and Space Administration
Glenn Research Center
Cleveland, Ohio 44135

Laura M. Cosgriff
Consultant
Lakewood, Ohio 44143

Bryan Harder and Dongming Zhu
National Aeronautics and Space Administration
Glenn Research Center
Cleveland, Ohio 44135

Richard E. Martin
Cleveland State University
Cleveland, Ohio 44115

Abstract

This study investigates the applicability of a novel noncontact single-sided terahertz electromagnetic measurement method for measuring thickness in dielectric coating systems having either dielectric or conductive substrate materials. The method does not require knowledge of the velocity of terahertz waves in the coating material. The dielectric coatings ranged from approximately 300 to 1400 μm in thickness. First, the terahertz method was validated on a bulk dielectric sample to determine its ability to precisely measure thickness and density variation. Then, the method was studied on simulated coating systems. One simulated coating consisted of layered thin paper samples of varying thicknesses on a ceramic substrate. Another simulated coating system consisted of adhesive-backed Teflon adhered to conducting and dielectric substrates. Alumina samples that were coated with a ceramic adhesive layer were also investigated. Finally, the method was studied for thickness measurement of actual thermal barrier coatings (TBC) on ceramic substrates. The unique aspects and limitations of this method for thickness measurements are discussed.

Introduction

Thermal barrier coatings (TBCs) and environmental barrier coatings (EBCs) are used to protect turbine engine components in high temperature or hostile environments (Ref. 1). Degradation of the TBCs or EBCs can lead to exposure of the substrate material to the high temperature, hostile engine environments resulting in damage to the substrate and component failure. Therefore, nondestructive evaluation (NDE) techniques that are capable of measuring the degradation and thickness of the coating materials are imperative to predicting remaining component life and failure (Refs. 1 to 3). TBCs and EBCs are applied to hot section engine components in a layer with a thickness that is typically less than 1 mm. Therefore, NDE techniques that are capable of characterizing coatings of thicknesses below 1 mm must be developed. Terahertz radiation wavelengths are on the order of 200 to 1500 μm (Refs. 4 to 7), making terahertz energy a good candidate for interrogation of coatings. Reflections occur at interfaces between materials with dissimilar dielectric properties (differences in indices of refraction). Metallic and

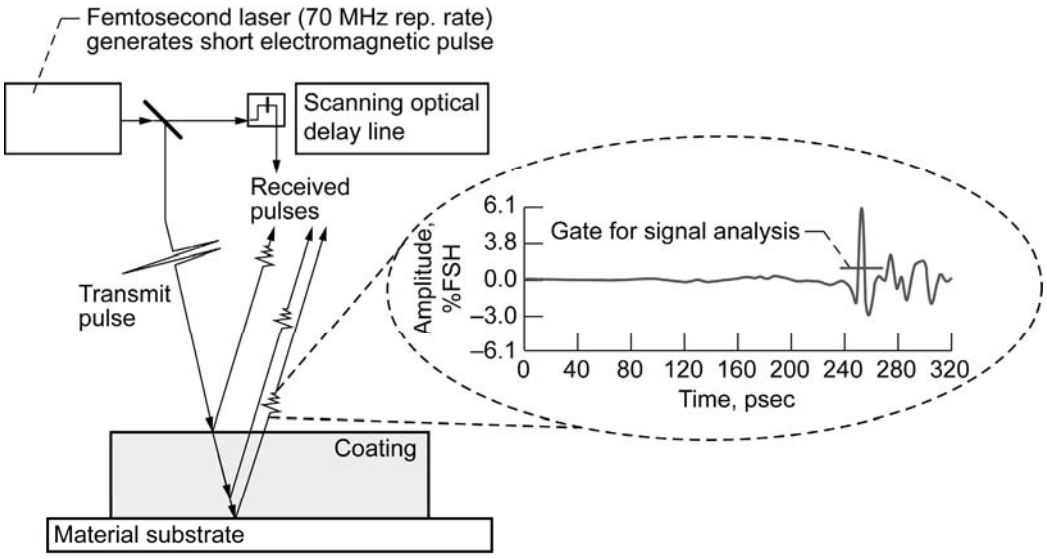

Figure 1.—Basic schematic diagram of reflection-mode terahertz methodology. Reflections will be received off of the various interfaces. The horizontal line over the echo shows the time gate typically used during signal processing.

conductive materials totally reflect terahertz waves, while nonpolar liquids, dielectric solids, and gases are partially transparent to terahertz energy. A significant advantage of terahertz waves for NDE is that they do not require a coupling medium (such as for ultrasonics) in order to interrogate a material. Continuous wave (narrowband) and pulsed (broadband) terahertz systems exist. This study is based on results from a reflection-mode broadband terahertz method with a collinear source-detector (transceiver) configuration shown schematically in Figure 1.

The use of terahertz for characterizing thickness and microstructure in coating materials has been previously investigated. The width and shape of the terahertz signal was utilized to monitor a thermally grown oxide layer and voids in TBCs that were approximately 300 μm thick (Ref. 8). A novel terahertz method to simultaneously characterize thickness and microstructural variation in thicker bulk materials was developed (Refs. 9 to 11). In the current study, the novel terahertz method was investigated for its ability to measure absolute thickness in the 300 to 1400 μm thickness range. Additionally, the use of the method to characterize global microstructural variation in one coating system independent of thickness is explored. The method was tested on a number of different coating systems as described in the experimental section. Limitations related to the use of this method on currently-manufactured TBC/EBC systems are discussed. Because TBCs typically consist of a heat-insulating (or dielectric) ceramic top coat and are often applied to a superalloy substrate, characterization with terahertz energy would be a very practical application.

Methodology

In this investigation, the conventional terahertz method of inspecting metal reflector-backed dielectric materials is taken advantage of to simultaneously provide microstructure-independent thickness (free of microstructure effects) measurements and images in coating materials. Figure 2 shows a schematic of the pulse-echo terahertz testing method and resulting waveforms.

A pulse-echo terahertz thickness measurement is made by sending terahertz energy via a transceiver (device that has both a transmitter and a receiver) into and through a dielectic coating backed by a material substrate that reflects the terahertz energy back to the transceiver. The terahertz transceiver is separated from the dielectric coating by an air path.

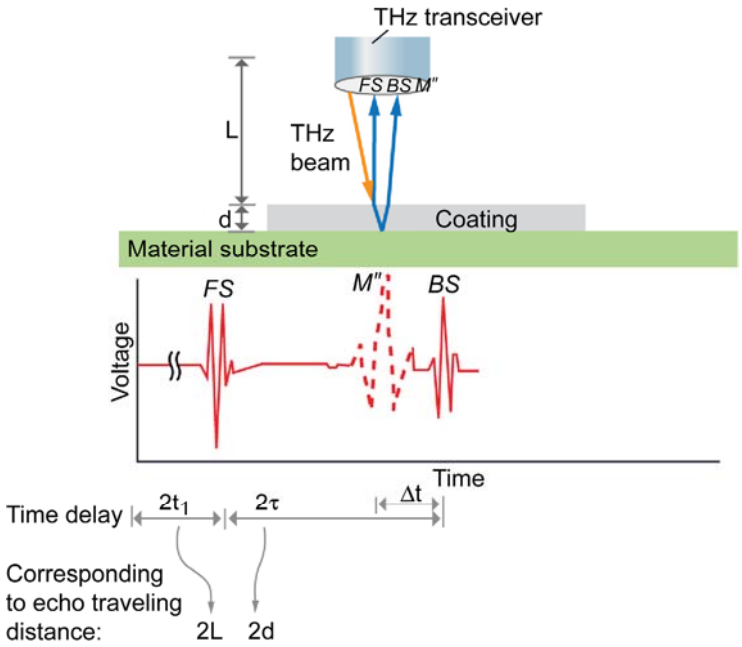

Figure 2.—Schematic of the pulse-echo testing and resulting waveforms. FS and BS occur with the coating present. M" occurs without the coating present.

Pulse-echo imaging involves mapping variations in the time-of-flight of a terahertz echo peak, or mapping the time delay between echoes off of a top surface of the coating (FS) and top surface of the underlying material substrate (BS) echoes, across a scanned sample. This scanning implementation concerns itself more with mapping thickness or global microstructural variation (such as physical density variation) as opposed to discrete flaw detection. Time delay between the front surface coating echo and material substrate top surface echo (2τ) is directly affected by thickness variation (d) and terahertz velocity (V) in the coating according to:

$$2\tau = \frac{(2d)}{V} \tag{1}$$

Here the designations 2τ and $2d$ (versus τ and d) are used since the terahertz echo travels through twice the coating thickness in the pulse-echo mode. Terahertz velocity is affected by variations in a volumetric microstructural property such as physical density, similar to the way ultrasonic velocity responds to microstructural variation (Refs. 12 to 14). Determining the relationship between terahertz velocity and density allows actual density maps to be obtained from velocity maps (Refs. 9 to 11). Variations in part thickness and/or lateral microstructural character will result in variations in maps of 2τ. Analogous to a complex number having real and imaginary parts, 2τ images can be thought of as having thickness and microstructural components if both thickness and microstructural variation are present.

Thickness Determination

The novel pulse-echo method described here for measuring coating thickness on an underlying material substrate uses time delay relationships between echoes off of the coating top surface (FS in Fig. 2), material substrate top surface with (BS in Fig. 2) and without (M" in Fig. 2) the coating present.

The following steps show how thickness (d) is determined without needing prior knowledge of coating velocity. With the coating present between the transceiver and the material substrate, the pulse that travels from the transceiver through the coating to the material substrate (equivalent to the coating back surface position or the interface of the coating and material substrate) and back to the transceiver is labeled *BS* and will be observed at time t' where:

$$t' = (2t_1 + 2\tau) \tag{2}$$

where $2t_1$ and 2τ are the pulse-echo time delays of the terahertz pulse from the transceiver to the coating front surface and from the coating front surface to the material substrate, respectively. Depositing the dielectric coating on the material substrate slows down the terahertz pulse as compared to its travel time in air. Thus, with the coating removed, the pulse that travels from the transceiver to the material substrate and back to the transceiver is labeled M" and will be observed at an earlier time t'' where:

$$t'' = \left(2t_1 + 2\frac{d}{c}\right) \tag{3}$$

where c is the velocity of terahertz energy in air and d is the air gap equal to the coating thickness. The velocity of light at standard temperature and pressure was used as in c in this investigation and is equal to 0.02997055434 cm/psec. Subtracting Equation (3) from Equation (2) gives:

$$t' - t'' = \Delta t = 2\tau - 2\frac{d}{c} \tag{4}$$

Rearranging Equation (4) to solve for coating thickness (d) gives:

$$d = \frac{c(2\tau - \Delta t)}{2} \tag{5}$$

which allows the calculation of absolute material thickness of the coating without prior knowledge of velocity. When this is extended to multiple measurements across the coating for imaging, sample microstructure variation effects are eliminated in the image allowing a true mapping of coating thickness variation. For conventional thickness mapping (rearranging Eq. (1) to solve for d), microstructure variation effects would corrupt the evaluation of thickness variation—thus the new methodology allows true characterization of thickness variation in a coating with non-uniform microstructure.

Velocity Determination

Similar logic can be used to solve for true velocity (V) in the coating as shown below. Rearranging Equation (1) to solve for $2d$ gives:

$$2d = (2\tau)V \tag{6}$$

Solving Equation (6) for d and substituting the result into Equation (4) gives:

$$\Delta t = 2\tau - \frac{2\tau V}{C} \tag{7}$$

Rearranging Equation (7) to solve for V gives:

$$V = c\left(1 - \frac{\Delta t}{2\tau}\right) \tag{8}$$

As seen from Equation (8), coating thickness (d) is not a variable in the equation. Thus, this method does not require prior knowledge of coating thickness. If extended to multiple measurements across the coating (imaging), coating thickness variation effects are eliminated in the image allowing a true picture of microstructural variation in the coating for types of microstructural variation (such as density variation) that correlate with and will be revealed by velocity variation. For conventional time-of-flight imaging (Eq. (1)), thickness variation effects would corrupt the evaluation of microstructural variation—thus the new methodology allows true thickness independent characterization of microstructural variations in the coating. Equation (9) shows how the terahertz velocity in a dielectric coating will be reduced fractionally from that in air by the factor:

$$\left(1 - \frac{\Delta t}{2\tau}\right) \tag{9}$$

A key point of the methodologies presented in this section are that both thickness-independent velocity and microstructure-independent thickness images can be derived from the same set of scan information. In practice, 2τ is experimentally obtained from the pulse-echo time delay between the first front surface of the coating surface (FS) and material substrate echo (BS). Δt is the pulse-echo time difference between the echo off the material substrate with and without the coating present, respectively. Either the time difference from peak locations or cross-correlation of the two echoes can be used to obtain the time delays.

Materials

Table 1 summarizes the substrate material—coating systems interrogated by THz in this study. Additional details on the material samples are described following the table.

TABLE 1.—MATERIAL SYSTEMS INTERROGATED BY THz

Material System	Substrate	Coating	Coating thickness range, μm	Coating density, g/cm^3	Coating porosity, percent	Notes
1	Metal plate	Silicon Nitride	3200 to 3500	5.9 to 6.1	2	Bulk sample on top of metal reflector plate
2	Nickel-base Superalloy	Paper	190 to 1440	~0.8	Undefined	Adhesive-backed “sticky notes”
3	Nickel-based Superalloy	Teflon	580 to 1200	2.2	Undefined	Adhesive-backed Teflon
4	Glass	Teflon	580 to 1200	2.2	Undefined	Adhesive-backed Teflon
5	Alumina	Sieved MgO-ZrO_2 based ceramic adhesive	489 to 514	~2.65 to 3.32	41	Sieved ceramic adhesive applied with a doctor blade
6	Alumina	As received MgO-ZrO_2 based ceramic adhesive	465 to 523	~1.74 to 1.98	48	As received ceramic adhesive applied with a doctor blade

Material System	Substrate	Coating	Coating thickness range, μm	Coating density, g/cm^3	Coating porosity, percent	Notes
7	Alumina	Sieved MgO-ZrO_2 based ceramic adhesive	489 to 514	~2.65 to 3.32	41	Sieved ceramic adhesive applied with a doctor blade
8	Alumina	Sieved MgO-ZrO_2 based ceramic adhesive and carbon black	417 to 521	~1.42 to 1.62	74	Sieved ceramic adhesive and carbon black applied with a doctor blade
9	Nickel-base superalloy	8YSZ	249 to 485	5.9 to 6.10	Undefined	8YSZ coating applied with an air plasma spray process

The first "coating" sample listed in Table 1 is a bulk silicon nitride dielectric sample which is approximately 3 by 1.5 cm. This silicon nitride sample, shown in Figure 3, has thickness varying from 3.2 to 3.5 mm and a small density variation of 2 percent due to porosity variation.

This sample was previously investigated using the novel terahertz method on another terahertz system (Ref. 9). It was important to be able to duplicate the previous results in order to validate the method on the system used in this study.

To simulate dielectric-coated samples, thin adhesive-backed paper samples (i.e., "sticky notes") were layered to create varying thicknesses on an electrically-conducting, nickel-based superalloy substrate. The total thicknesses of the layered sticky notes varied from 190 to 1440 μm. This is the second material system listed in Table 1.

The third and fourth material systems on Table 1 represented another set of simulated coatings consisting of adhesive-backed Teflon. First, rectangles consisting of three different thicknesses from approximately 580 to 1200 μm of Teflon were adhered to the nickel-based superalloy substrate. A schematic illustrating the layout of the three thicknesses is shown in Figure 4.

Then, to further investigate the method's capabilities in interrogating dielectric coatings on dielectric substrates, Teflon rectangles were adhered to a glass substrate.

Two sets of three 1 by 1 in. alumina substrates with a MgO-ZrO_2 based ceramic adhesive coating were also evaluated. The first set of three samples was created to have uniform material/density but different thicknesses and is the fifth material system listed in Table 1. To create the coatings for the first set of samples with the same density, the larger grains were first sieved from the MgO-ZrO_2 based ceramic powder using a 100 mesh sieve allowing grains smaller than the mesh opening of 6 mil (0.152 mm) to pass through. The sieved powder was then combined with water and applied to the surface of the alumina substrate using a doctor blade. After the coating was cured in a 126 °C (259 °F) oven for several hours, the coated samples were placed in a 700 °C (1292 °F) degree oven to remove any impurities. The coatings were then polished, attempting to create a uniform surface area on each coated sample to be evaluated with terahertz. Coating thickness ranged from ~480 to 493 μm on the first sample, ~492 to 519 μm on the second sample, and ~663 to 682 μm on the third sample.

A second set of three 1 by 1 in. alumina substrates with a MgO-ZrO_2 based ceramic adhesive coating samples were manufactured with different densities but approximately the same thickness in order to evaluate the terahertz method for characterizing microstructural variation in coatings. These are the 6, 7, and 8 material systems listed in Table 1. First, the same sieved MgO-ZrO_2 based ceramic adhesive coating used for material system 5 was applied to an alumina substrate using a doctor blade. Then, carbon black was added to the sieved MgO-ZrO_2 based ceramic adhesive to create additional porosity in the coating. To create a third material/density difference, the as-received, unsieved MgO-ZrO_2 based ceramic powder was combined with water and applied to the alumina substrate. After the coatings cured in a 126 °C (259 °F) oven for several hours, the coated samples were placed in a 700 °C (1292 °F) degree

oven to eliminate the carbon and any additional impurities. The coatings were then polished to approximately the same thickness, attempting to create a uniform surface area on each coated sample to be evaluated with terahertz. Coating porosities were found using Archimedes' method to be 48 percent for the as received ceramic adhesive, 41 percent for the sieved ceramic adhesive, and 74 percent for the sieved ceramic adhesive with carbon black.

Finally, 1.9 by 1.9 cm square Nickel-based superalloy substrates were coated with 8-YSZ (yttria-stabilized zirconia) using an air plasma spray (APS) process. Eight samples with coating thicknesses varying from 249 to 485 μm were investigated with terahertz. This is the ninth material system listed in Table 1.

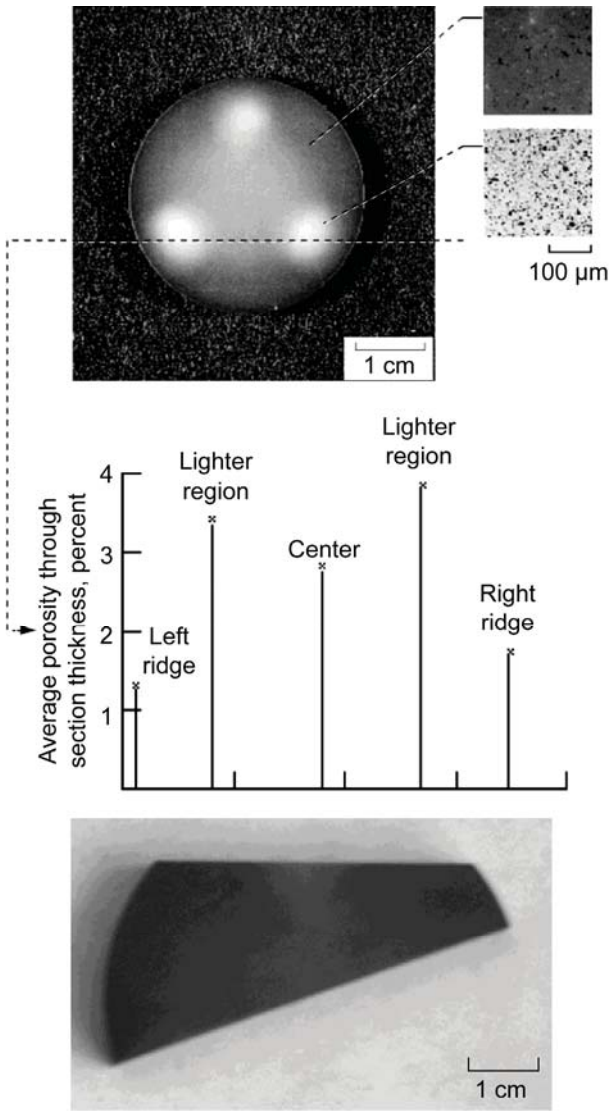

Figure 3.—Silicon nitride wedge sectioned from a disk containing lower than average pockets of density and an edge to center density gradient. The wedge thickness varies left to right from 3.2 to 3.5 mm.

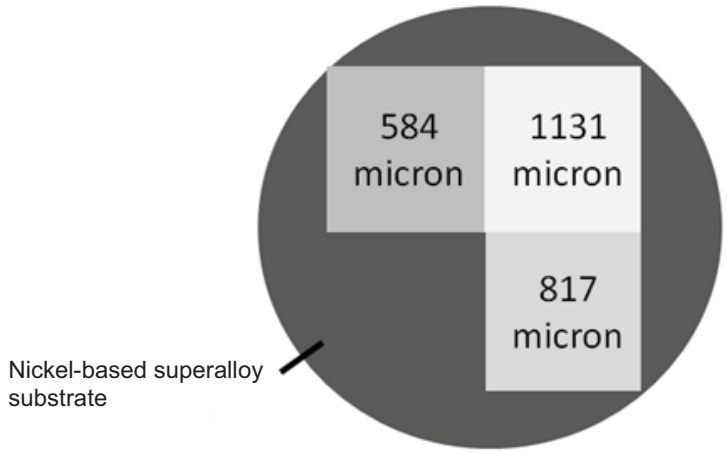

Figure 4.—Schematic of the Teflon rectangular samples adhered to a circular Nickel-based superalloy substrate disk. The thickness of each Teflon section is shown in the schematic.

TABLE 2.—DIELECTRIC CONSTANTS, k
[At standard temperature and pressure, relative to vacuum.]

Material	k
Vacuum	1
Air	1.0059
Paper	2
Silicon Nitride	4.2
Teflon	2.1
Glass	3.7 to 10
Alumina	4.5
Cement (powder)	5 to 10
8YSZ	24
Water (68 °F)	80.4

Table 2 lists the room temperature dielectric constants for some of the coating and substrate materials used in this study (Refs. 15 to 17). Materials with a low dielectric constant, close to 1, are transparent or near transparent to terahertz energy, while materials with dielectric constants larger than 1 will reflect some fraction of the incident terahertz energy. As the dielectric constant approaches that of water (80.4), more of the Terahertz energy is reflected. Highly conductive materials, such as metals, have very high dielectric constants and reflect all of the terahertz energy. The dielectric constants for a vacuum, air and water are included in the table for reference. The dielectric constant for the nickel-based superalloy is unavailable because it is such a conductive material, reflecting all of the Terahertz energy. A difference in dielectric constant, or dielectric mismatch, between two layered materials, will result in some terahertz energy being reflected from and some being transmitted into the layer that the terahertz energy is incident upon. The greater the mismatch, the greater the amount of reflected energy.

Terahertz Scanning

Two scans were obtained for each sample studied with the THz system shown in Figure 5 before and after applying a simulated or actual coating material to the material substrate.

The THz signalis generated by the pulsed THz controller, which contains the laser, power supplies, and other components of the system. A lensed, collinear reflection transceiver was used to send and receive the THz signal into the dielectric coating material. Each acquired waveform consisted of 400 points over an 80 psec time window. The resulting time domain resolution is 0.2 psec per acquisition point. The THz

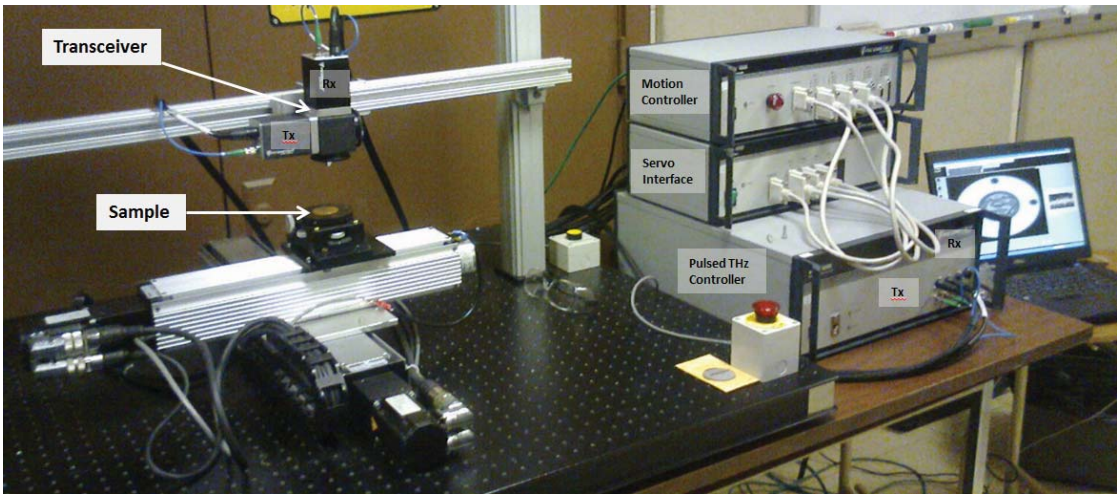

Figure 5.—Photograph of the THz system utilized in this study.

bandwidth of the pulse is 0.01 to 2 THz. To maximize the signal amplitude, the transceiver was focused at the substrate at the lens focal length of 76.2 mm (3 in.). The focal spot size was 2 mm which is approximately the limit of lateral resolution.

For each material system interrogated, a baseline scan of the underlying material substrate without the coating present, yielding the M" echo, and a scan with the coating present, containing the FS and BS echoes, was acquired. For example, the bulk silicon nitride wedge sample was placed on an aluminum plate within the scan system hardware. A baseline scan was obtained from the aluminum plate, without the silicon nitride sample present, and yielded the M" echo. A second scan was then performed with the sample placed on the aluminum plate to obtain the FS and BS echoes.

For the coated samples, first, a baseline scan from the uncoated material substrate was obtained and yielded the M" echo. The second scan with the coatings present provided the FS and BS echoes. The FS echo reflected off the top surface of the coating, while the BS echo represents a reflection off of the material substrate top surface. The scan and step increments were 0.5 by 0.5 mm.

The time delays 2τ and Δt were measured using the negative peak times (valleys) of the FS, M", and BS echoes (Fig. 2). For the samples in this study, FS, M", and BS echoes were in phase with each other and had distinct single negative peaks. Waveform data from the substrate only and substrate with coating scans were used to create a "Fused" data file using the NDE Wave and Image Processor (Ref. 18). This merged data contains the FS, BS, and M" at each scan location and is used for all subsequent data analysis.

Results and Analysis

Silicon Nitride Wedge

To validate the current terahertz system and to determine the novel THz method's ability to measure thickness and density variation, the silicon nitride wedge sample with thickness and density variation was scanned using the methodology described above. Figure 6 shows the fused THz waveform with the front surface (FS), back surface (BS), and M" echoes labeled.

The results in Figure 7 show that the terahertz thickness measurements agree with the thicknesses as measured with a micrometer. In fact, the THz thickness measurements were within 4 percent of the micrometer measured thickness. In addition, these results were in agreement with previously published terahertz thickness results on the same sample (Ref. 9), hence verifying the method for thickness measurement. The echoes obtained for this material are of extremely high signal-to-noise ratio with well-formed valleys from which time-of-flight was extracted.

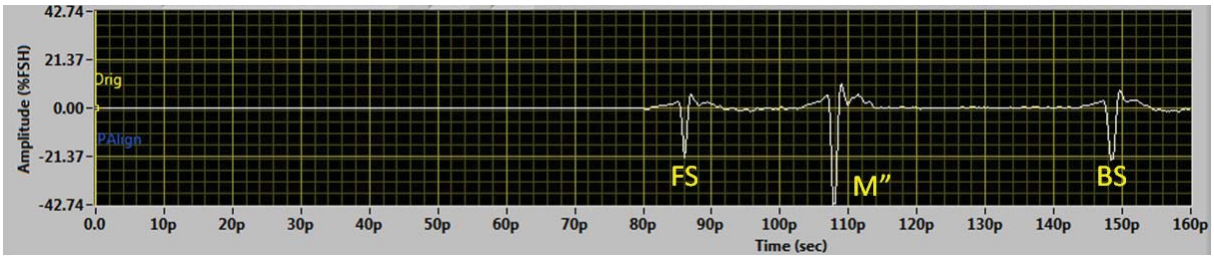

Figure 6.—Fused THz waveform from the two scans of the silicon nitride sample with the front surface (FS), back surface (BS), and M" echoes.

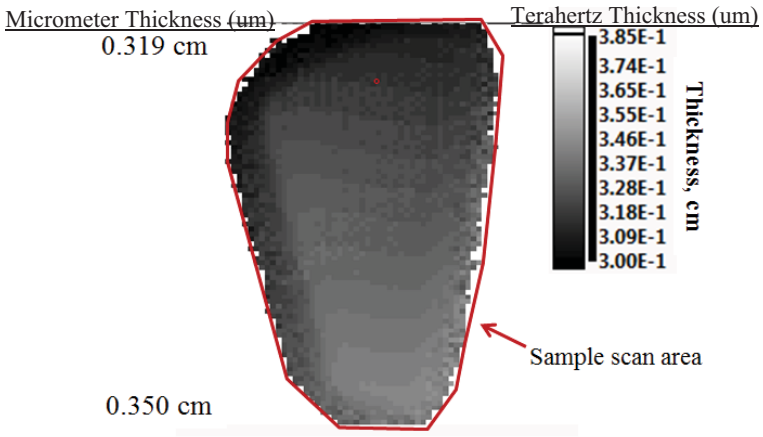

Figure 7.—Terahertz thickness map from the silicon nitride ceramic sample. Thickness as measured with a micrometer is shown on the left. Thickness as measured with THz is shown in the scale on the right.

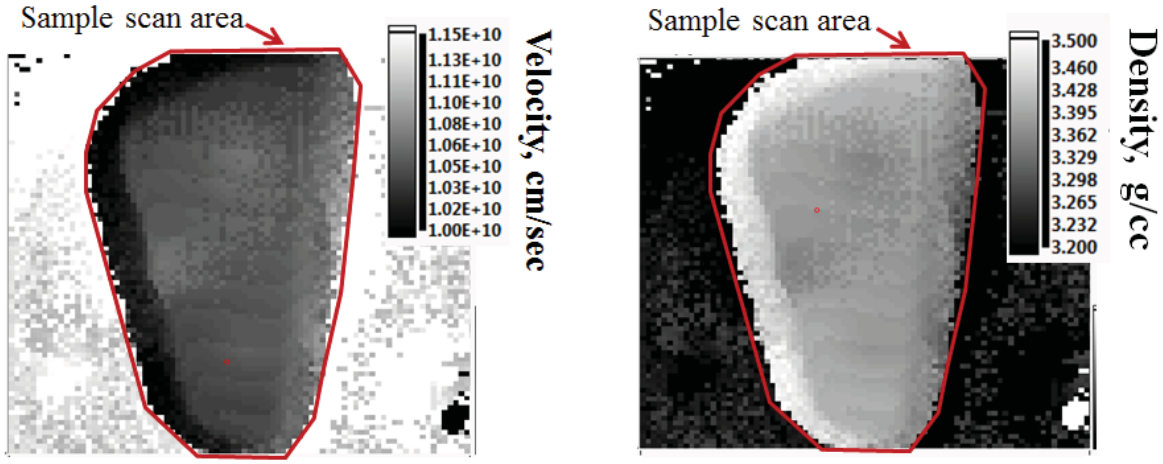

(a) Velocity map (b) Density map

Figure 8.—Velocity map (a) and the density map (b) for the silicon nitride wedge. Density map obtained from the relationship between density and terahertz velocity in silicon nitride from prior work (Ref. 10).

Figure 8 shows the THz velocity map (a) and the terahertz-derived density map (b) for the silicon nitride wedge. The velocity values were converted to density values using the best linear curve fit reported in previous work (Ref. 10). The density variation shown in Figure 8(b) corresponds well with the variations shown by optical microscopy (Fig. 3). These density results also agree with previously published results (Ref. 10), thus validating the method for thickness and density variation characterization.

Layered Paper on Ceramic Substrate

The novel THz scanning method was next applied to simulated coating systems consisting of layered thin paper samples (i.e., “sticky notes”) of varying thicknesses on a ceramic substrate. The thicknesses of the layered paper samples, as measured by a micrometer, ranged from 190 to 1440 µm. Three thicknesses of layered paper were applied to the ceramic substrate for an individual scan. This was done for three different thickness ranges of papers to provide three sets of scan results. A typical fused waveform from the layered paper on a nickel-based superalloy material systems is shown with the FS, M”, and BS echoes labeled in Figure 9. Since the paper samples all had uniform microstructure, it was expected that paper coating velocity would be almost constant regardless of the coating thickness. The THz thickness and velocity results from the THz scan with the thickest set of layered paper sections are shown in Figure 10.

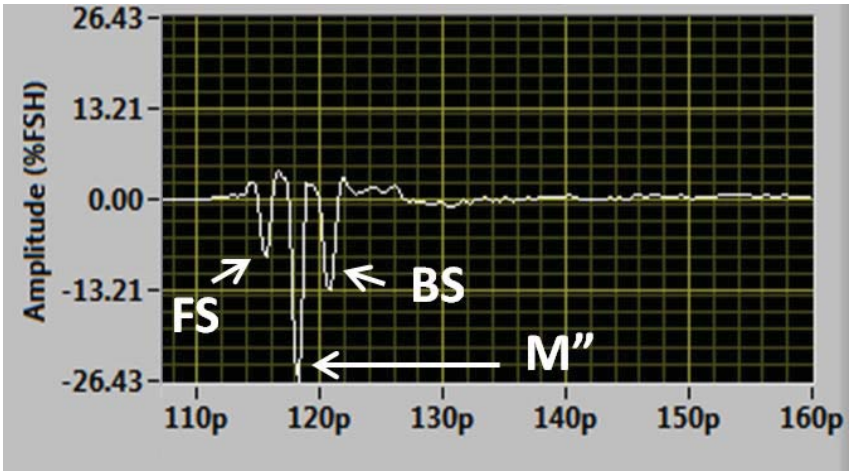

Figure 9.—Typical fused waveform from the 490 µm thick layered paper on a nickel-based superalloy with the front surface (FS), back surface (BS), and uncoated substrate (M”) echoes labeled.

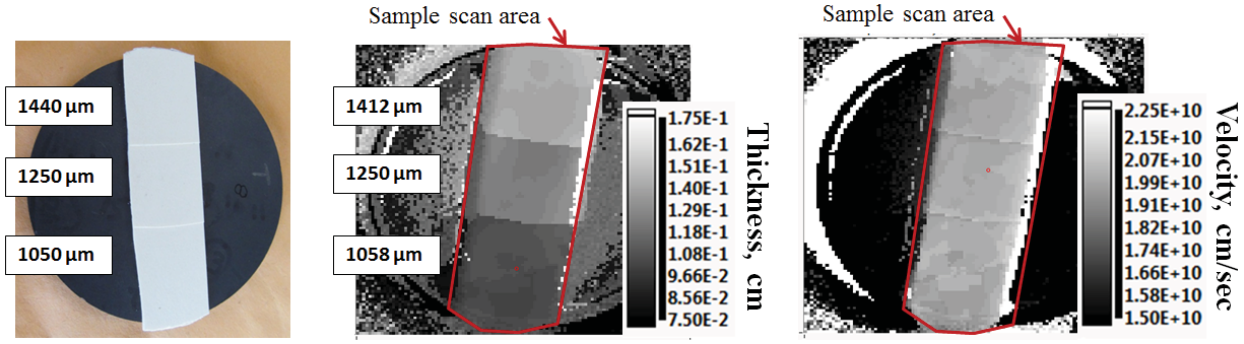

(a) Photo of disk with layered paper

(b) THz thickness

(c) THz velocity map

Figure 10.—Photograph and THz results from the paper layers ranging from 1050 to 1440 µm thickness on a nickel-based superalloy. Thickness values shown are the mean calculated from five locations (center and four quadrants for each thickness).

TABLE 3.—THICKNESS MEASUREMENTS OF LAYERED PAPER ON A NICKEL-BASED SUPERALLOY SUBSTRATE
[All values shown are the mean of five locations (center and four quadrants for each thickness).]

Micrometer measured thickness, µm	THz thickness, µm	Percent difference, thickness	THz velocity, cm/sec
1440	1412	1.9	2.00E+10
1250	1250	0.0	2.02E+10
1050	1058	–0.8	2.01E+10
480	520	–8.3	2.07E+10
380	419	–10.3	2.10E+10
290	311	–7.2	2.02E+10
390	498	–27.7	2.52E+10
290	396	–36.6	2.61E+10
190	318	–67.4	3.12E+10

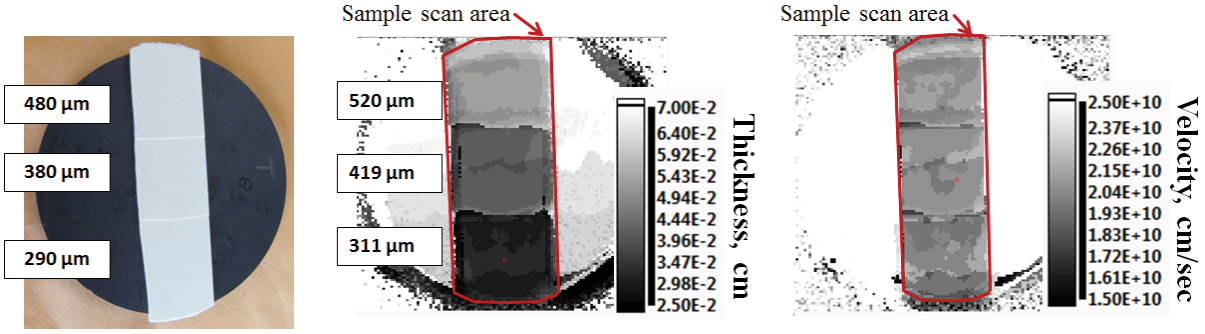

(a) Photo of disk with layered paper

(b) THz thickness map

(c) THz velocity map

Figure 11.—Photograph and THz results from the paper layers ranging from 290 to 480 µm thickness on a nickel-based superalloy. Thickness values shown are the mean calculated from five locations (center and four quadrants for each thickness).

Table 3 summarizes the THz results from all the layered paper samples with each listed measurement representing the average of five locations. The percent difference in thickness between micrometer-measured and terahertz-measured thickness was calculated using the formula:

$$\text{Percent Difference} = \frac{100 * (A - T)}{A} \tag{11}$$

where A is the micrometer measured thickness and T is the THz thickness.

The mean THz thicknesses from the three thickest paper layers were 1058, 1250, and 1412 µm, which represents a –0.8, 0, and 1.9 percent, difference from the micrometer measured thicknesses of 1050, 1250, and 1440 µm. The THz thickness and velocity results from another set of layered paper are shown in Figure 11.

The nearly-uniform gray scale color of the velocity maps in Figures 10 and 11 indicate that the THz velocity is relatively uniform as expected, regardless of thickness. The variation of the THz velocities found from the 1050, 1250, and 1440 µm thicknesses is low with the total standard deviation approximately 0.5 percent of their means. However, as the thickness of the three paper layers scanned decreased, the percent difference between all of the velocities increased and the standard deviation of the THz velocities also increased. For the thinnest paper layers of 190, 290, and 390 µm, the percent difference was as high as 67.4 percent and the standard deviation of the THz velocities from the three thicknesses was 11.7 percent of the mean of the three THz velocity values. This is likely related to FS, BS, and M" waveforms interference reducing the precision of true peak (valley) detection. Interpolation of the waveforms by a factor four times (increasing point density by four times) was used in an attempt to improve the precision of valley detection for better thickness accuracy but it did not help.

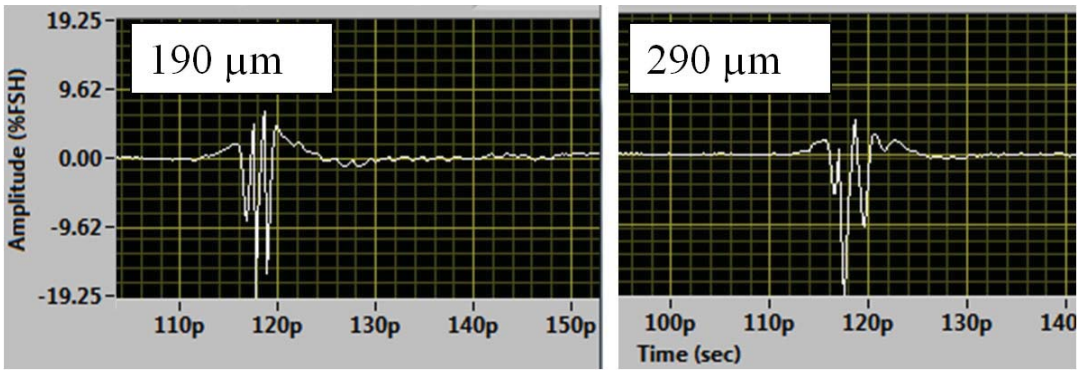

(a) Waveform from the 190 µm thick section (b) Waveform from the 290 µm thick section

Figure 12.—Fused THz waveforms from the thinnest paper layers on a ceramic substrate illustrating the decrease in separation between FS, BS, and M" echoes. The amplitude scale is the same for both waveforms.

Figure 12 shows the decrease in separation between the echoes of the fused waveform. It became difficult to unambiguously detect the valley needed for time-of-flight extraction. Therefore, analysis of these layered samples helped define a practical thickness limit of 350 µm for the method. This limit will depend upon the velocity of terahertz in a material (lower velocity provides greater FS and BS echo separation), but it was consistently observed for the samples in this study. A minimum coating thickness of 350 µm provides enough separation in time between FS and BS and prevents overlap of FS, BS, and M" echoes during the gating, fusing and analysis process. When analyzing layers thicker than 350 µm, the accuracy improves considerably.

Teflon on Glass and Nickel-Based Superalloy

Adhesive-backed Teflon was adhered to glass and to a Nickel-based superalloy in the next set of tests with the novel terahertz method. A glass substrate, representing a dielectric/insulating material, and a Nickel-based superalloy substrate, representing a conductive material, was used to compare the capabilities of the system for investigating material systems having dielectric versus conductive substrates. The results shown here represent Teflon thicknesses measured with a micrometer ranging from approximately 590 to 1100 µm. A fourth Teflon thickness of approximately 330 µm was also measured. However, this thickness was deemed too thin to evaluate as its inclusion in the analysis caused large percent differences in the thickness measurements and large variations in the velocity measurements. This result further defined the practical thickness limit of 350 µm for the THz method discussed above. For thicknesses below 350 µm, interference between front surface and back surface echoes resulted in difficulty obtaining accurate time-of-flight values needed for velocity and thickness calculation.

The fused waveform from Teflon on a glass substrate is shown in Figure 13. The FS, M", and BS echoes are labeled, along with an additional echo further in time, labeled fixture echo. The fixture echo is thought to be the echo from the interface of the back surface of the glass and the support fixture where the Teflon and glass material system sample is placed and did not influence the thickness or velocity analysis or the calculations. More of the Terahertz penetrated the dielectric glass material than has been observed in other material systems. This makes sense since glass is non-electrically-conducting. Figure 14 shows the THz thickness and velocity scan results from the Teflon adhered to the glass substrate.

As shown in Table 4, THz thickness measurements of the Teflon layers on the glass substrate were within 3 to 5 percent of the measured thickness. Each thickness and velocity value listed in the table represents an average of five locations in each thickness region. Velocity varied across all of the samples by ~1.5 percent, regardless of thickness.

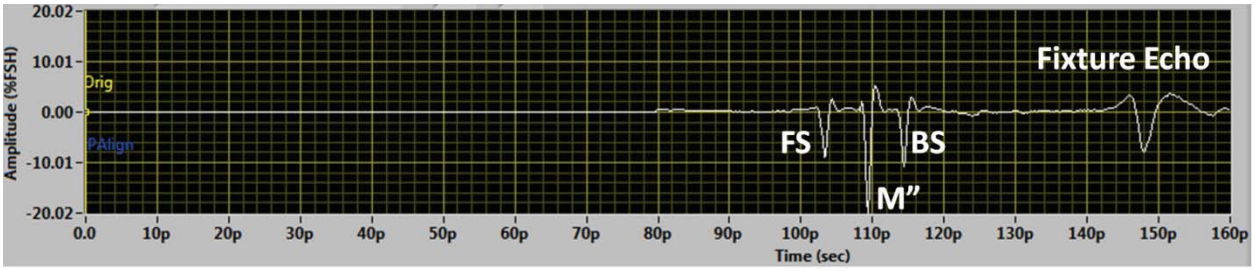

Figure 13.—Fused THz waveform from the 1136 μm thick section of adhesive-backed Teflon on a glass substrate with the FS, M”, BS, and an additional fixture echo labeled.

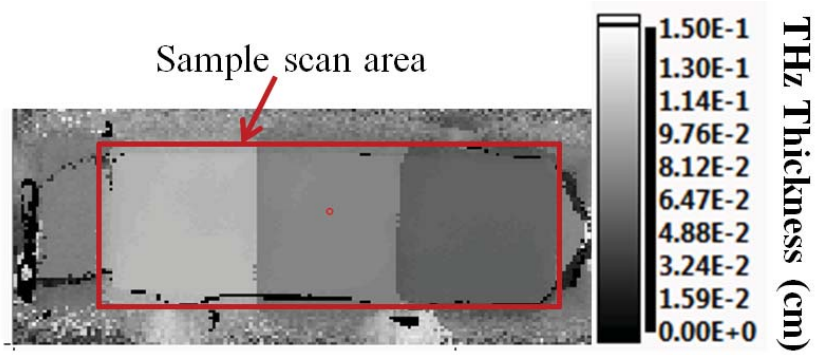

(a) THz thickness map

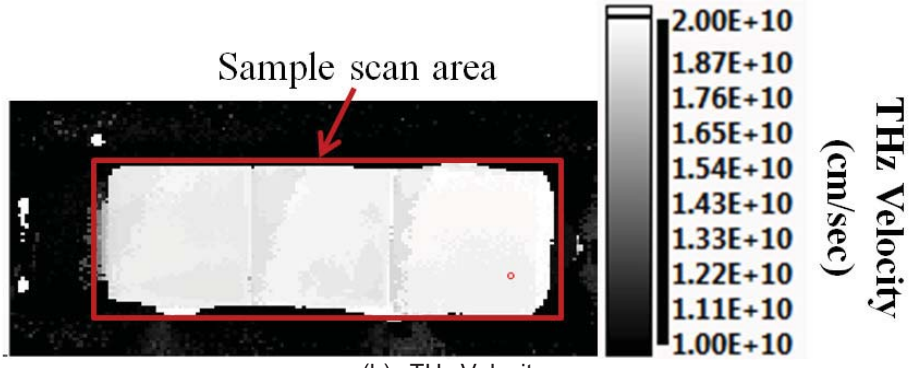

(b) THz Velocity map

Figure 14.—Thickness map (a) and velocity map (b) for adhesive-backed Teflon on a glass substrate.

TABLE 4.—THICKNESS MEASUREMENTS OF TEFLON ON GLASS SUBSTRATE
[All values shown are the mean of five locations (center and four quadrants for each thickness).]

Micrometer measured thickness, μm	THz thickness, μm	Percent difference thickness	THz velocity, cm/sec
588	568	3.4	1.93E+10
818	790	3.4	1.94E+10
1136	1078	5.1	1.96E+10

A representative fused waveform from Teflon on the nickel-based superalloy is shown in Figure 15 with the resulting THz thickness map shown in Figure 16.

As shown in Table 5, THz thickness measurements of the Teflon layers from the nickel-based superalloy substrate were within 4 percent of the thickness measured with a micrometer. Each thickness and velocity value listed in the table represents an average of five locations in each thickness region. The image in Figure 16(a) shows that the thickness was uniform over each region. The image in Figure 16(b) shows that the THz velocity and material density was also uniform.

It appears that the THz results from the two systems with material substrates having different dielectric properties are very similar. Although the amplitude of the THz signal was slightly larger from the nickel-based superalloy substrate versus the glass substrate, the percent differences between the micrometer-measured and THz-measured thicknesses were both ≦ ~5 percent. Velocity varied across all of the samples by ~3.5 percent, regardless of thickness.

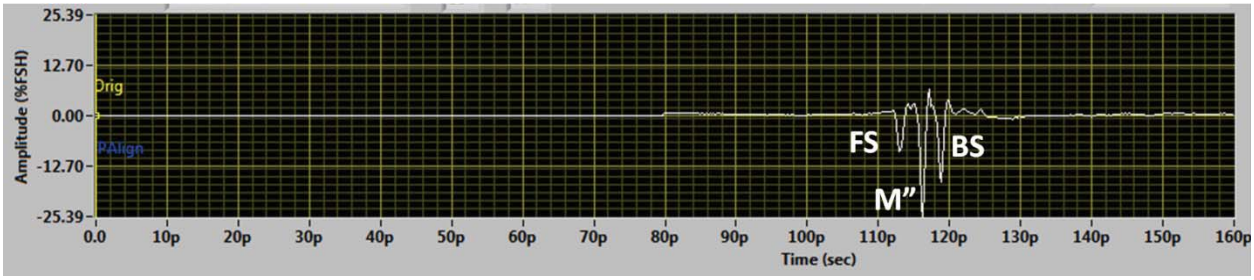

Figure 15.—Fused THz waveform from the 1128 μm thick section of adhesive-backed Teflon on nickel-based superalloy with the FS, M", and BS echoes labeled.

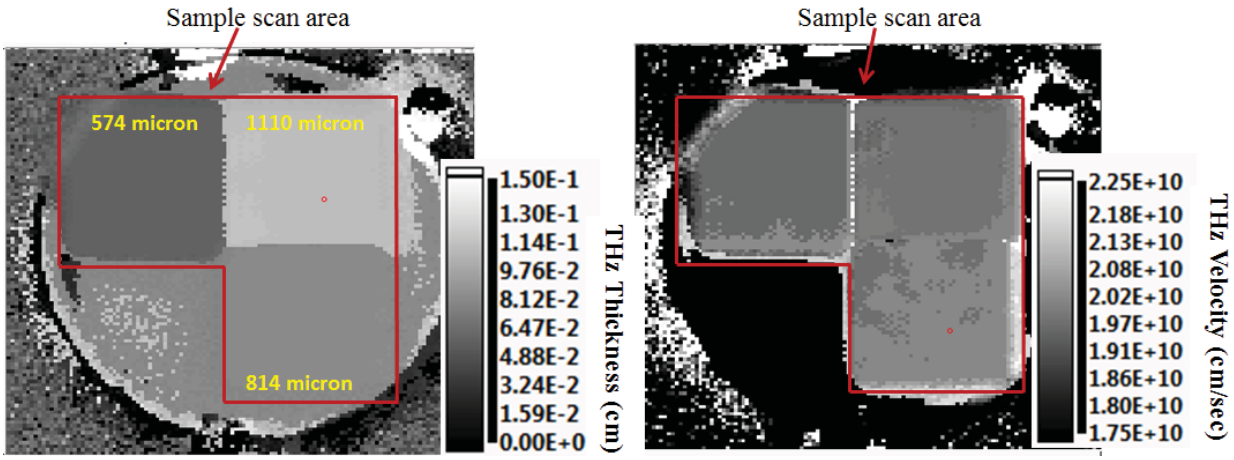

(a) Thickness map (b) Velocity map

Figure 16.—Thickness map (a) and velocity map (b) from the adhesive-backed Teflon samples on a conductive nickel-based superalloy substrate.

TABLE 5.—THICKNESS MEASUREMENTS OF TEFLON ON NICKEL-BASED SUPERALLOY
[All values shown are the mean of five locations (center and four quadrants for each thickness).]

Micrometer measured thickness, μm	THz thickness, μm	Percent difference thickness	THz velocity, cm/sec
596	574	3.7	1.95E+10
814	814	0.0	2.02E+10
1128	1110	1.6	1.98E+10

Ceramic ($MgO\text{-}ZrO_2$) Adhesive on Alumina Substrate

To further investigate the capabilities of the method to characterize thickness and material density on actual coatings, ceramic adhesive was applied to alumina substrates. For the first set of samples the thickness was varied, while attempting to keep the material/density the same (Table 1, material 5). For the second set of samples attempts were made to keep the thickness uniform, while varying the material density (Table 1, materials 6 to 8).

Figure 17 shows the THz thickness and velocity maps from the ceramic adhesive with varying thickness. Due to machining difficulties, a uniform thickness was not obtained for these samples. Therefore, instead of averaging the thicknesses from the center and four quadrants, as was done for the analysis of the previous coating systems, single thickness and velocity values from the five individual locations were calculated. Table 6 lists the THz thickness and velocity measurements from the five locations on each of the three samples.

THz thickness measurements were obtained with percent differences between micrometer- and THz-measured thicknesses up to 31 percent. The THz velocities varied by 13 percent, perhaps indicating that the microstructures were not uniform. Figure 18 shows a waveform with the FS, M", and BS echoes labeled. The peak from the BS echo is not as sharp as it is for some other materials (like Teflon, as shown in Fig. 15). The dullness of the BS echo peak may make it difficult to find the correct time of flight measurements for calculating thickness.

Figure 19 shows the THz thickness and velocity maps from the ceramic adhesive with intentionally-varying density. Attempts were made to create a uniform thickness from sample to sample, but due to machining difficulties, a uniform thickness was not achievable. Therefore, single thickness and velocity values from the center and the four quadrant locations were calculated individually. Table 7 summarizes these THz thickness and velocity measurements from these samples. The estimated porosity is included on the table for reference.

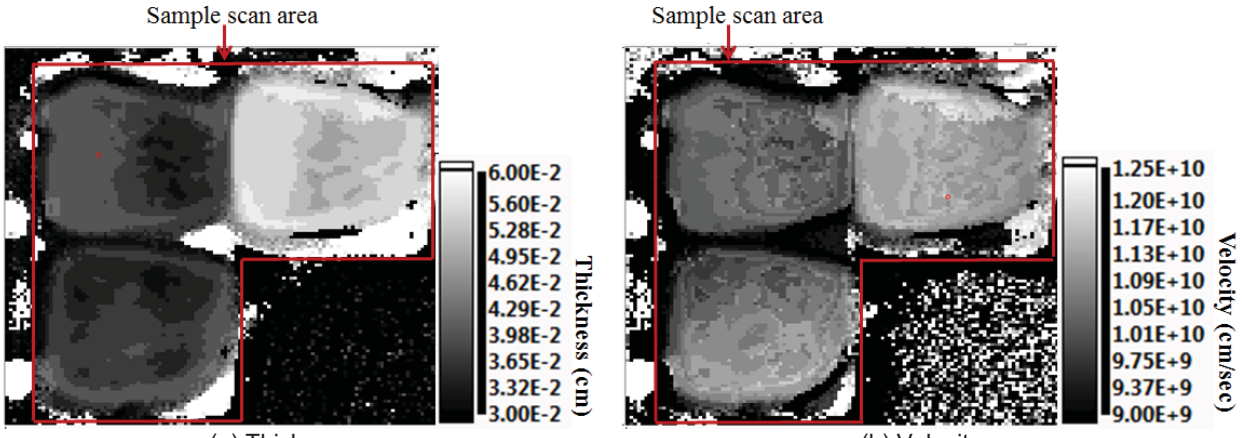

(a) Thickness map (b) Velocity map

Figure 17.—THz thickness map (a) and velocity map (b) from the ceramic adhesive with varying thicknesses but the same material (sieved ceramic adhesive).

TABLE 6.—THz THICKNESS AND VELOCITY MEASUREMENTS OF CERAMIC ADHESIVE OF VARYING THICKNESS

Micrometer measured thickness, µm	THz thickness, µm	Percent difference thickness	THz velocity, cm/sec
487	582	30.2	1.00E+10
482	612	23.2	1.13E+10
480	552	22.9	1.09E+10
493	462	31.0	1.07E+10
486	522	23.9	1.10E+10
518	400	22.8	1.06E+10
519	400	22.9	1.03E+10
512	370	27.7	1.03E+10
492	340	30.9	1.00E+10
495	340	31.3	1.03E+10
663	550	17.0	1.13E+10
681	550	19.2	1.13E+10
671	490	27.0	1.13E+10
666	520	21.9	1.11E+10
682	550	19.4	1.09E+10

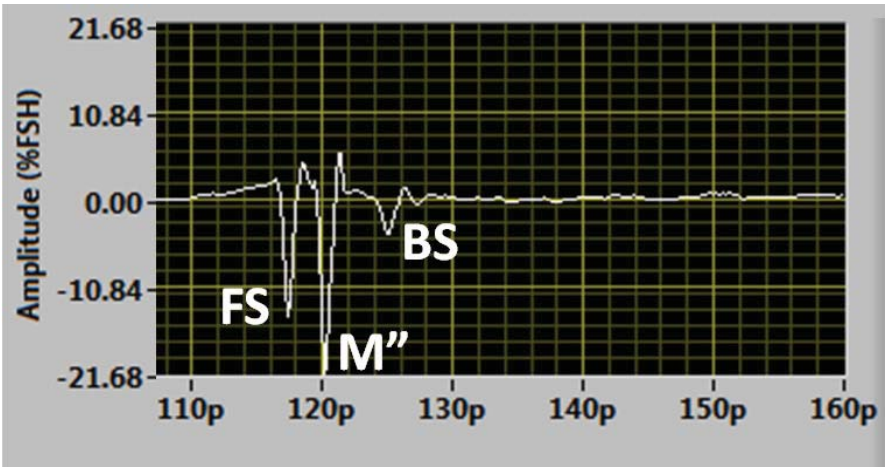

Figure 18.—Typical fused waveform from the sieved ceramic adhesive on alumina.

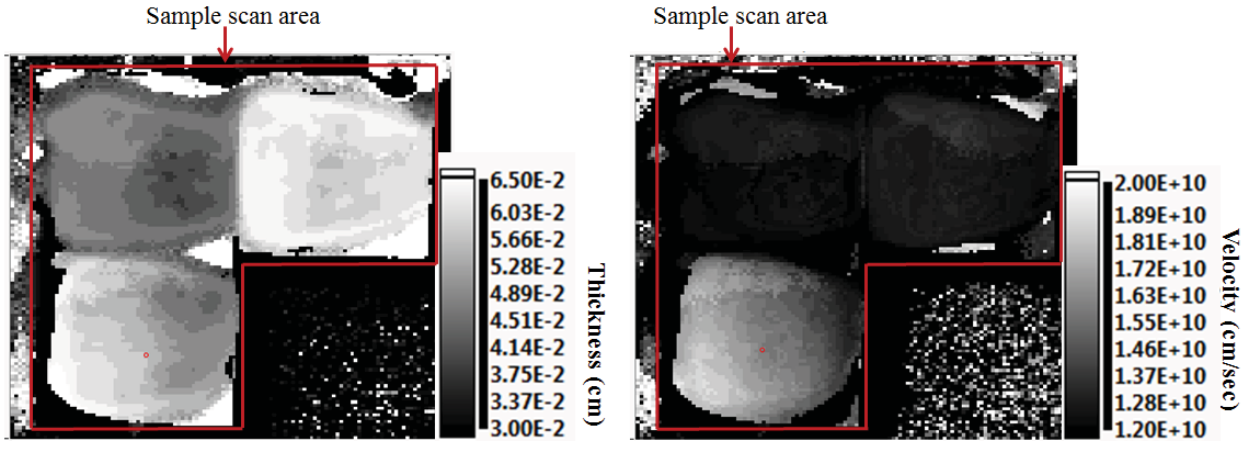

(a) Thickness map (b) Velocity map

Figure 19.—THz thickness map (a) and velocity map (b) from the ceramic adhesive with varying material/density but the similar thicknesses.

TABLE 7.—THICKNESS MEASUREMENTS OF VARYING CERAMIC ADHESIVE ON AN ALUMINA SUBSTRATE

Micrometer measured thickness, μm	THz thickness, μm	Percent difference thickness	THz velocity, cm/sec	Estimated porosity, percent
489	428	12.5	1.30E+10	41
504	458	9.1	1.25E+10	41
504	428	15.1	1.33E+10	41
510	428	16.1	1.30E+10	41
514	458	10.9	1.30E+10	41
465	428	8.0	1.63E+10	48
488	428	12.3	1.46E+10	48
489	338	30.9	1.45E+10	48
505	458	9.3	1.58E+10	48
523	488	6.7	1.42E+10	48
417	338	18.9	1.45E+10	74
428	338	21.0	1.45E+10	74
475	368	22.5	1.45E+10	74
480	368	23.3	1.52E+10	74
521	309	40.7	1.58E+10	74

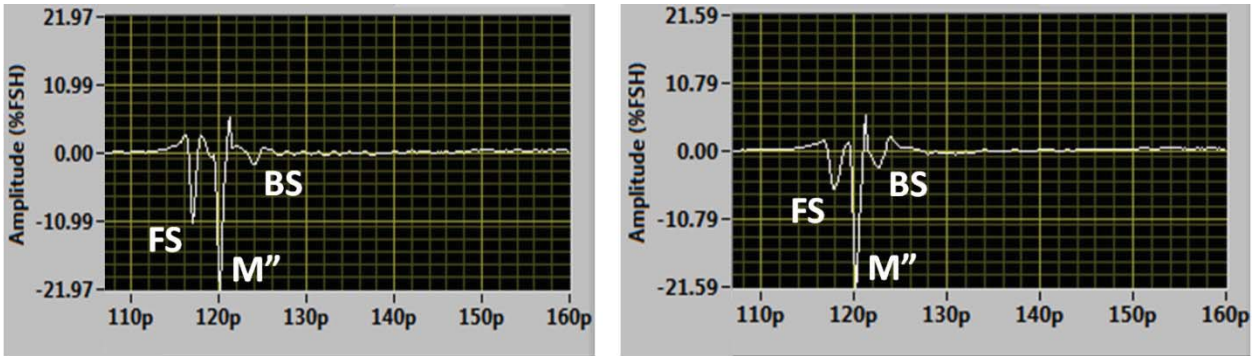

(a) As received ceramic adhesive (b) Sieved ceramic adhesive with carbon

Figure 20.—Typical fused waveforms from (a) the as-received ceramic adhesive on alumina (estimated porosity 48 percent) and (b) the sieved ceramic adhesive and carbon black on alumina (estimated porosity 74 percent).

Figure 20 shows the fused waveforms from the as-received ceramic adhesive on alumina (estimated porosity 48 percent) and the sieved ceramic adhesive and carbon black on alumina (estimated porosity 74 percent).

Thickness differences between micrometer- and terahertz-measured thicknesses ranged from 7 percent up to 40 percent. The coating with the highest porosity of 74 percent also had the highest percent differences in thickness ranging from 19 to 41 percent. Figure 20 shows representative waveforms from these two material systems with the FS, M”, and BS echoes labeled. For the material system with the highest porosity, the valley from the BS echo (shown in Fig. 20(b)) is not as sharp as it is for some other materials (like Teflon, as shown in Fig. 15). The dullness (wideness and flatness) of the BS echo valley may make it difficult to find the correct time of flight measurements for calculating velocity. The average THz velocity for the material system with the sieved ceramic coating with an estimated porosity of 41 percent was 1.30E+10 cm/sec. This represents the average of the first five locations listed in Table 7. The average THz velocity for the material system with the as-received ceramic coating with an estimated porosity of 48 percent was 1.51E+10 cm/sec which was ~13 percent greater than the mean velocity for the 41 percent coating illustrating the greater velocity for a coating with more air as would be expected. However, this trend did not remain consistent when comparing the 48 percent porous coating with the 74 percent porous coating. The average THz velocity for the material system with the estimated porosity of 74 percent was 1.49E+10 cm/sec, approximately the same as for the 48 percent porous coating.

8YZS Coated Nickel-Based Superalloy Samples

The method was studied on actual thermal barrier coating (TBC) systems consisting of 8YSZ (Yttria-stabilized Zirconia) coating applied to a nickel-based superalloy. The coating thicknesses, as measured by a micrometer, ranged from 249 to 485 μm. Table 8 lists the THz thickness and velocity results from the eight 8YSZ-coated nickel-based superalloy samples.

For the samples with the thinnest layers of coating ranging from 249 to 267 μm, the percent difference from the THz thickness measurements ranged from 28 to 51 percent with the larger percent difference associated with the thinnest coating. These results further confirmed the result suggesting a practical inspection limit of 350 μm that was observed with the layered paper samples and the adhesive-backed Teflon. When considering only the coating thicknesses > 400 μm, the micrometer- and THz-measured thicknesses differed by 20 to 30 percent which was higher than consistently observed for the other coating systems. Again, considering only the coating thicknesses > 400 μm, the velocities varied by only 3.9 percent which is consistent with that expected for a uniform coating.

The 8YSZ coated samples were notably rougher than the other samples utilized in this investigation. Surface roughness measurements were collected from some of the 8YZS -coated samples and the Teflon-coated samples to determine if some of the large thickness error variation could be explained by the surface variation. The average roughness, denoted by R_a, was calculated over a 2.5 by 1.9 mm area on each sample using the following formula:

$$R_a = \frac{1}{MN}\sum_{j=1}^{M}\sum_{k=1}^{N}\left|Z_{jk}\right| \tag{12}$$

where Z_{jk} is the height of each pixel after the zero mean is removed and M and N are the x and y dimensions of the area. The surface roughness was calculated for the Teflon sample as 448.49 nm (or 0.448 μm), which represents 0.04 percent of the full thickness of 1128 μm. A three-dimensional surface roughness image for the Teflon sample is shown in Figure 21.

In comparison, the surface roughness from an 8YSZ coated sample identified was calculated as 16.27 μm, which represents 3 percent of the micrometer-measured thickness of 483 μm. For the 267 μm thick coating, R_a was calculated as 14.61 μm, which represents 5 percent of the micrometer measured thickness of 267 μm. So, approximately 5 percent of the percent difference of the thickness may be explained by the surface roughness of the coating. A three-dimensional surface roughness image for the 483 μm thick 8YSZ coating is shown in Figure 22 with coating thickness peaks being 78 μm above the zero mean and the valleys being 76 μm below the zero mean.

TABLE 8.—THICKNESS MEASUREMENTS OF 8YZS COATED NICKEL-BASED SUPERALLOY SAMPLES

[All values shown are the mean of five locations (center and four quadrants for each thickness).]

Micrometer measured thickness, μm	THz thickness, μm	Percent difference, thickness	THz velocity, cm/sec
267	342	–28.1	9.56E+09
254	364	–43.3	1.08E+10
485	611	–26.0	9.27E+09
483	592	–22.6	9.25E+09
249	375	–50.6	1.10E+10
249	372	–49.4	1.08E+10
452	566	–25.2	9.19E+09
447	577	–29.1	9.38E+09

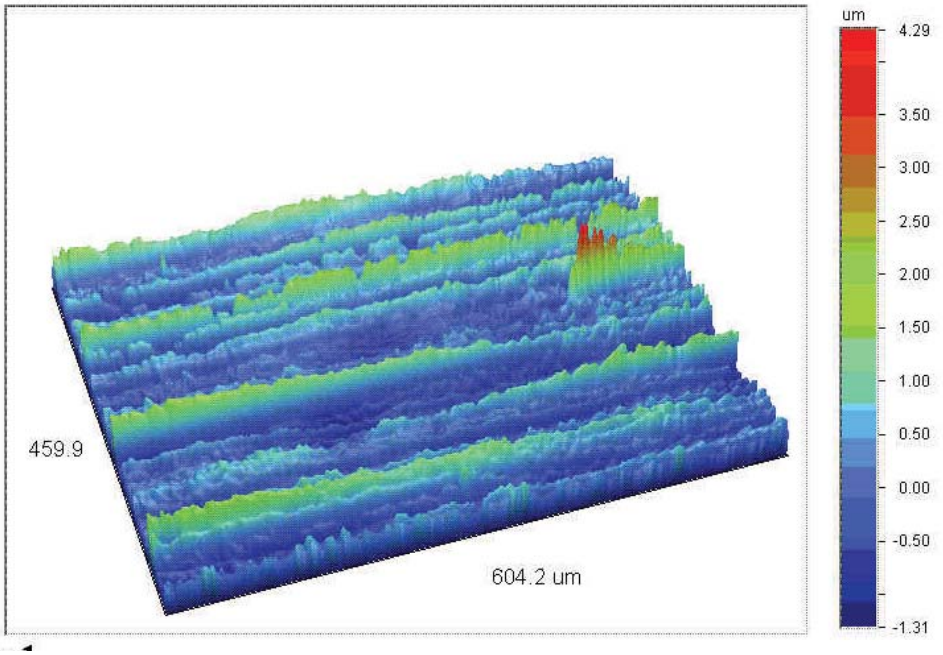

Figure 21.—A three-dimensional surface roughness image from a Teflon-coated sample.

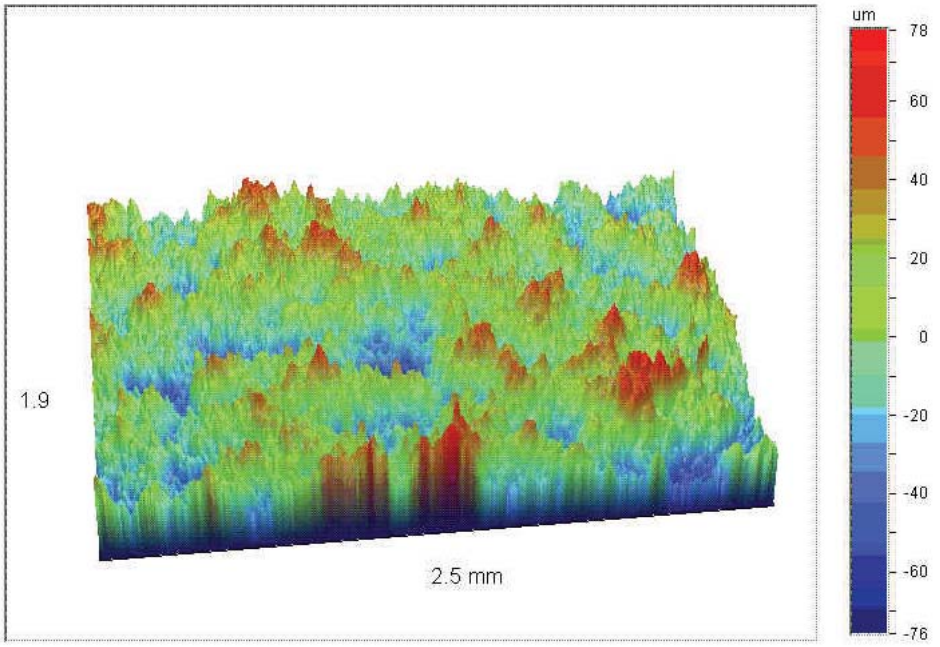

Figure 22.—A three-dimensional surface roughness image from an 8YSZ-coated sample.

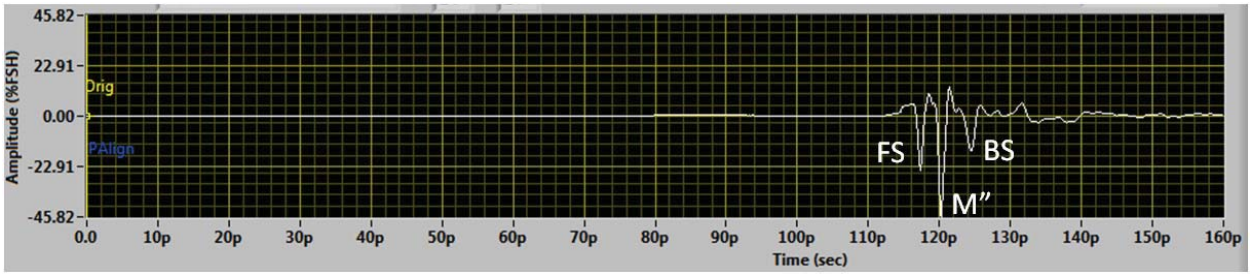

Figure 23.—A fused waveform from one of the 8YSZ-coated samples with the FS, M”, and BS echoes labeled.

The accuracy of micrometer measurements for the 8YSZ samples is questionable due to the thickness nonuniformity of the coating. The micrometer measurement will always be an overestimate because it measures the highest peak within the micrometer gauge, introducing some additional error in the thickness measurements. In addition, it is likely that the surface roughness caused scatter in the THz signal which would lower the signal to noise ratio and change the morphology of the front and back surface echoes. Figure 23 shows the fused waveform from the first 8YSZ-coated sample listed in Table 8. The morphology of the BS echo peak is not well defined and is wider than the BS echo for the Teflon coating system shown in Figure 15.

Conclusion

The applicability of a novel noncontact single-sided terahertz electromagnetic measurement method for measuring coating thickness in dielectric coating systems having either dielectric or conductive substrate materials was investigated. The method does not require prior knowledge of the material properties (terahertz velocity) in the coating material. However, terahertz measurement is required prior to coating deposition. The dielectric coatings ranged from approximately 300 to 1400 μm in thickness. First, the method was validated on a bulk dielectric sample to determine the method's ability to precisely measure thickness and density variation. Then, the method was studied on simulated coating systems. One simulated coating system consisted of thin layers of paper samples on a ceramic substrate. Another simulated coating system consisting of adhesive-backed Teflon was adhered to electrically-conductive and dielectric substrates. This method was proven applicable for a dielectric coating on a dielectric substrate. Thus, it can be utilized where eddy current methods for thickness measurement cannot be used. Finally, the method was studied for thickness measurement of actual thermal barrier coatings (TBC) on conducting ceramic substrates.

Coating thicknesses measured with terahertz were within 0 to 10 percent of the actual coating thicknesses measured by micrometer for the simulated coating systems but showed much greater deviation from actual thicknesses for the rough-surfaced TBC-coated samples. It is thought that the rough surface and variable microstructure of the TBC coatings caused waveform distortion resulting is less accuracy of the method. It was found that use of this terahertz thickness measurement method is practical for coatings greater than approximately 350 μm (depending on the terahertz velocity in the coating). Below that thickness, interference between front surface and back surface echoes resulted in difficulty obtaining accurate time-of-flight values needed for velocity and thickness calculation.

References

1. Vaβen, Robert, Yutaka Kagawa, Ramesh Subramanian, Paul Zombo, and Dongming Zhu, *Testing and evaluation of thermal-barrier coatings*, MRS Bulletin, 37 (2012) 911–916.
2. Ghosn, Louis, Dongming Zhu, *Thermal Barrier and Protective Coatings to Improve the Durability of a Combustor under a Pulse Detonation Engine Environment,* 48th AIAA/ASME/ASCE/AHS/ASC Structures, Structural Dynamics, and Materials Conference 23–26 April 2007, Honolulu, Hawaii.
3. Zhu, Dongming and Robert Miller*, Development of Advanced Low Conductivity Thermal Barrier Coatings*, International Journal of Applied Ceramic Technology, 1 (1) 86–94, 2004.
4. R.A. Cheville, M.T. Reiten, J. O'Hara, and D.R. Grischkowsky, "THz time domain sensing and imaging," R.J. Hwu, and L.W. Dwight, eds. (SPIE, 2004), pp. 196–206.
5. D.M. Mittleman, R.H. Jacobsen, and M.C. Nuss, "T-ray imaging," IEEE J.Sel. Tops. Quantum 2(3), 679–692 (1996).
6. L. Duvillaret, F. Garet, and J.-L. Coutaz, "Highly precise determination of optical constants and sample thickness in terahertz time-domain spectroscopy," Appl. Opt. 38(2), 409–415 (1999).
7. T. Yasui, T. Yasuda, K.-i. Sawanaka, and T. Araki, "Terahertz paintmeter for noncontact monitoring of thickness and drying progress in paint film," Appl. Opt. 44(32), 6849–6856 (2005).
8. Chen, Chia-Chu, Dong-Joon Lee, Tresa Pollock, and John F. Whitaker, *Pulsed-terahertz reflectometry for health monitoring of ceramic thermal barrier coatings*, Optics Express, 19 (4) 2010.
9. Roth, D.J., Seebo, J.P., and Winfree, W.P., "Simultaneous Noncontact Precision Imaging of Microstructural and Thickness Variation in Dielectric Materials Using Terahertz Energy," *Materials Evaluation*, Vol. 66, No. 3, March 2008. pp. 325–331.
10. Roth, Don J., J.P. Seebo, and W.P. Winfree, *Simultaneous Noncontact Precision Imaging of Microstructural and Thickness Variation in Dielectric Materials using Terahertz Energy*, NASA/TM—2008-214997.
11. D.J. Roth, US Patent# 7,876,423 B1 entitled "Simultaneous Noncontact Precision Imaging of Microstructural and Thickness Variation in Dielectric Materials Using Terahertz Energy," Jan. 2011.
12. Generazio, E.R., Roth, D.J., and Stang, D.B., "Ultrasonic Imaging of Porosity Variations Produced During Sintering," *J. Am. Ceram. Soc*, vol. 72, no. 7, 1989.
13. Roth, D.J., Stang, D.B., Swickard, S.M., DeGurire, M.R., and Dolhert, L.E., "Review, Modeling, and Statistical Analysis of Ultrasonic Velocity—Pore Fraction Relations in Polycrystalline Materials," *Materials Evaluation*, vol. 49, no. 7, July 1991, pp. 883–888.
14. Roth, D.J., Kiser, J.D., Swickard, S.M., Szatmary, S., and Kerwin, D., "Quantitative Mapping of Pore Fraction Variations in Silicon Nitride Using an Ultrasonic Contact Scan Technique," *Research in Nondestructive Evaluation*, vol. 16, no. 3, 1995.
15. Lide, D.R., ed. (2000). *CRC Handbook of Chemistry and Physics* (81st ed.). Boca Raton (FL): CRC Press.
16. Dielectric Constants of Materials (2007). Clipper Controls. http://www.clippercontrols.com/pages/Dielectric-Constant-Values.html
17. S.H. Jeong, I.S. Bae, Y.S. Shin, S.-B. Lee, H.-T. Kwak, J.-H. Boo, *Physical and electrical properties of ZrO_2 and YSZ high-k gate dielectric thin films grown by RF magnetron sputtering*, Thin Solid Films 475 (2005) 354–358.
18. Roth, D.J., "Demonstration of an NDE Post-Processing Software Tool Developed at NASA Glenn Research Center," Presentation and Proceedings of ASNT Fall 07, November 12–16, Las Vegas, NV.